JOURNAL OF PETROLOGY | VOLUME 49 | NUMBER 4 | PAGES 841–855 | 2008 | doi:10.1093/petrology/egn007

Seismic Properties of Anita Bay Dunite: an Exploratory Study of the Influence of Water

YOSHITAKA AIZAWA[1,2†], AUKE BARNHOORN[1§], ULRICH H. FAUL[1‡], JOHN D. FITZ GERALD[1], IAN JACKSON[1]* AND ISTVÁN KOVÁCS[1]

[1]RESEARCH SCHOOL OF EARTH SCIENCES, AUSTRALIAN NATIONAL UNIVERSITY, CANBERRA, ACT 0200, AUSTRALIA
[2]INSTITUTE FOR STUDY OF THE EARTH'S INTERIOR, OKAYAMA UNIVERSITY, MISASA, TOTTORI, 682-0193, JAPAN

RECEIVED DECEMBER 8, 2006; ACCEPTED FEBRUARY 11, 2008
ADVANCE ACCESS PUBLICATION MARCH 4, 2008

As a pilot study of the role of water in the attenuation of seismic waves in the Earth's upper mantle, we have performed a series of seismic-frequency torsional forced-oscillation experiments on a natural (Anita Bay) dunite containing accessory hydrous phases, at high temperatures to 1300°C and confining pressure (P_c) of 200 MPa, within a gas-medium high-pressure apparatus. Both oven-dried and pre-fired specimens wrapped in Ni–Fe foil within the (poorly) vented assembly were recovered essentially dry after 50–100 h of annealing at 1300°C followed by slow staged cooling. The results for those specimens indicate broadly similar absorption-band viscoelastic behaviour, but with systematic differences in the frequency dependence of strain-energy dissipation Q^{-1}, attributed to differences in the small volume fraction of silicate melt and its spatial distribution. In contrast, it has been demonstrated that a new assembly involving a welded Pt capsule retains aqueous fluid during prolonged exposure to high temperatures—allowing the first high-temperature torsional forced-oscillation measurements under high aqueous fluid pore pressure P_f. At temperatures >1000°C, a marked reduction in shear modulus, without concomitant increase in Q^{-1}, is attributed to the widespread wetting of grain boundaries resulting from grain-scale hydrofracturing and the maintenance of conditions of low differential pressure $P_d = P_c - P_f$. Staged cooling from 1000°C is accompanied by decreasing P_f and progressive restoration of significantly positive differential pressure resulting in a microstructural regime in which the fluid on grain boundaries is increasingly restricted to arrays of pores. The more pronounced viscoelastic behaviour observed within this regime for the Pt-encapsulated specimen compared with the essentially dry specimens may reflect both water-enhanced solid-state relaxation and the direct influence of the fluid phase. The scenario of overpressurized fluids and hydrofracturing in the Pt-encapsulated dunite specimen may have some relevance to the high Q^{-1} and low-velocity zones observed in subduction-zone environments. The outcomes of this exploratory study indicate that the presence of water can have a significant effect on the seismic wave attenuation in the upper mantle and provide the foundation for more detailed studies on the role of water.

KEY WORDS: *seismic wave attenuation; water; dunite; hydrous mineral; shear modulus; viscoelasticity; olivine; grain-scale hydrofracturing*

INTRODUCTION

Seismological observations have revealed that the propagation of seismic waves in the Earth's mantle is significantly affected by viscoelastic processes, causing attenuation and frequency dependence (dispersion) of wave speeds (e.g. Kanamori & Anderson, 1977; Anderson & Hart, 1978). It is widely accepted that such viscoelastic processes are associated with the motion of crystal defects such as grain boundaries and dislocations in rocks at high temperatures and/or the stress-induced redistribution of fluids including melt (e.g. Nowick & Berry, 1972; Minster & Anderson, 1981; Karato & Spetzler, 1990; Jackson, 2007). However, further understanding of these processes has been limited by lack of direct measurements of viscoelasticity for mantle materials such as olivine at high temperature and seismic frequency.

In recent years the application of seismic-frequency torsional forced-oscillation methods to fine-grained polycrystalline olivine has become feasible and revealed that elastic behaviour breaks down at sufficiently high temperatures, even in melt-free material, resulting in stronger

*Corresponding author. Telephone: +61 2 6125 2498. Fax: +61 2 6125 8253. E-mail: Ian.Jackson@anu.edu.au
†Present address: Japan Manned Space Systems Corporation, MY Bldg., 1-1-26, Kawaguchi, Tsuchiura, Ibaraki 300-0033, Japan.
‡Present address: Department of Earth Sciences, Boston University, Boston, MA 02215, USA.
§Present address: Faculty of Geosciences, Department of Earth Sciences, Utrecht University, PO Box 80021, 3508 TA Utrecht, The Netherlands.

temperature sensitivity of wave velocity and associated attenuation (Tan *et al.*, 1997; Gribb & Cooper, 1998; Jackson *et al.*, 2002). These viscoelastic effects vary systematically with grain size and have been attributed to elastically and/or diffusionally accommodated grain-boundary sliding (Cooper, 2002; Jackson *et al.*, 2002; Faul *et al.*, 2004).

A pronounced effect of water on viscoelastic processes has been suggested (Karato & Jung, 1998; Karato, 2003) based on the analogy with its effect on creep, in which a trace amount of water significantly weakens olivine-rich rocks (Carter & Avé Lallemant, 1970; Chopra & Paterson, 1984; Karato *et al.*, 1986; Mei & Kohlstedt, 2000). Water weakening of olivine aggregates in creep is currently interpreted in terms of increased concentrations of point defects, such as Si and/or Mg/Fe vacancies, resulting in enhanced rates of ionic diffusion and dislocation climb (e.g. Mei & Kohlstedt, 2000; Kohlstedt, 2006; Walker *et al.*, 2007). However, the influence of water on the microstrain viscoelasticity has not yet been investigated experimentally.

This exploratory study serves to test two hypotheses: (1) that water can be retained in the specimen at high temperatures (up to 1150°C) during the long duration (50–100 h) forced-oscillation experiments; (2) that the presence of water has an effect on the seismic wave attenuation in mantle materials. Here we report the first seismic-frequency measurements of the influence of water on seismic wave dispersion and attenuation in polycrystalline olivine. For these exploratory experiments we chose a naturally occurring material (see Jackson *et al.*, 1992)—in this case a relatively fine-grained, hydrated but unserpentinitized, dominantly olivine rock from Anita Bay (New Zealand), previously used in the studies that first demonstrated the effect of water on creep behavior of olivine (Chopra & Paterson, 1981, 1984). We measured both prefired and initially untreated specimens (either wrapped in Ni–Fe foil or Pt-encapsulated) to isolate the effect of water.

EXPERIMENTAL PROCEDURES

Specimen preparation

Starting material

The natural dunite specimen from Anita Bay, New Zealand is a 30 cm diameter boulder that consists primarily of olivine (>90 vol. % of composition Fo_{93}, Chopra & Paterson, 1981), orthopyroxene and chromite but also contains minor amounts of hydrous phases, in the form of chlorite, tremolite and thin sheets of talc. Cylindrical samples cored from the same boulder were used in the studies by Chopra & Paterson (1981, 1984) and Faul & Jackson (2007). It is compositionally banded with a strong mineral lineation but foliation is weak and no crystallographic preferred orientation is indicated, consistent with previous studies of Anita Bay material (Turner, 1942; Wood, 1972). A trimodal grain-size distribution is evident with an overall average grain size of 100 μm. The fine-grained fraction (20–30% of thin-section area) has a grain size around 20 μm and consists mainly of lineation-parallel domains of orthopyroxene mixed with olivine. The fine-grained material is crack free and has straight grain boundaries. The medium-grained fraction (50–60%) consists almost exclusively of ~100 μm sized olivine grains with no undulose extinction and minor intragranular fracturing. Olivine–olivine grain boundaries in these regions are distinctly serrated (Fig. 1). Large porphyroblasts of olivine and orthopyroxene (up to 8 mm in size and elongated parallel to the lineation) form 10–20% of the sample. They display undulose extinction and at least two generations of fractures.

Cylindrical specimens were cored parallel to the lineation and precision ground to 11·5 mm in diameter and 30 mm in length. All four samples were cored in close proximity to each other. The density of a representative oven-dried specimen was determined by the Archimedean method involving immersion in ethanol to be $3{\cdot}2986(2) \times 10^3\,kg/m^3$. This is 99·7% of the theoretical density of olivine (Fo_{93}) (Chopra & Paterson, 1984), in accordance with a dunite composition.

Heat treatment prior to mechanical testing

In preparation for mechanical testing the rock specimens were either simply oven-dried (at 110°C; runs 1066 and 1093) or fired at 1200°C for 20 h (runs 1055 and 1086) in a controlled oxygen fugacity furnace using a gas mixture comprising equal partial pressures of CO and CO_2, yielding $\log_{10} f_{O2}(Pa) \sim -6$ (Muan & Osborn, 1965). Based on the weight loss on ignition, the initial volatile content of the as-received rock was estimated to be 0·20 wt %, which is within the range of previous estimates (0·18 ± 0·02 wt %) (Chopra & Paterson, 1981).

Infrared spectroscopy for [H_2O] determination

The water content [H_2O] was determined by unpolarized IR spectroscopy on doubly polished disks nominally of ~0·5 mm thickness cut from the cylindrical dunite specimens (Tan *et al.*, 2001). For determination of the average concentration of water in the bulk specimens, an aperture of at least 4 mm diameter was employed, whereas for spot analyses, for example within olivine porphyroblasts, an aperture of 70 μm diameter was selected. The concentration of molecular water, contained mainly in fluid inclusions, and responsible for the broad absorption band at wavenumber ν of 3000–3700 cm^{-1} (Fig. 2), was estimated from the absorbance measured at 3400 cm^{-1} with an absorption coefficient of 8·1 cm^{-1} $(mol/l)^{-1}$ (Rossman, 1988).

Hydroxyl chemically bound within the olivine structure is responsible for sharp IR absorption peaks within the

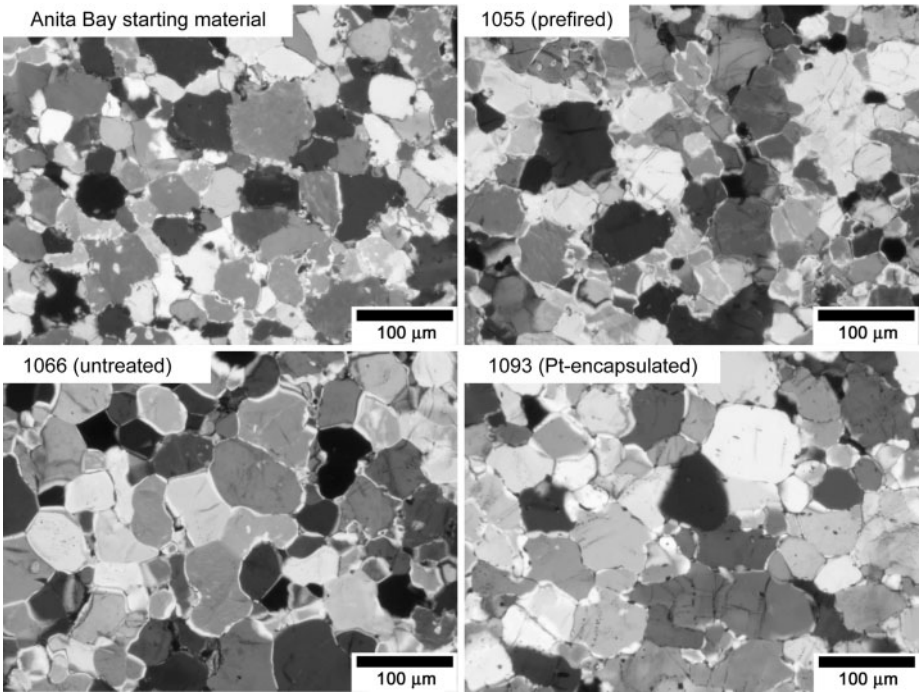

Fig. 1. Transmitted-light micrographs (with crossed polarizers) of grain-boundary microstructures. Comparison of those for the pre-fired specimen (1055) and the starting material shows very little textural evolution with similar average grain size and serrated grain boundaries. In specimen 1066, subject to progressive *in situ* dehydration at 1300°C, water has apparently enhanced the textural evolution with clear evidence of grain growth and of smoother grain boundaries. The Pt-encapsulated specimen 1093 displays an intermediate degree of textural development attributed to the substantially lower maximum temperature (1150°C).

wavenumber ranges 3280–3380 and 3450–3510 cm^{-1}, superimposed upon the broad-band absorption attributed to fluid inclusions (Fig. 2d). To facilitate comparison with the water concentrations reported by Zhao *et al.* (2004) for similar conditions, their procedure was adopted for the estimation of [H_2O], notwithstanding emerging indications that it may systematically overestimate water concentrations estimated from unpolarized spectra (Kovács *et al.*, 2008; Sambridge *et al.*, 2008). First, we calculated the integrated absorbance associated with such peaks normalized to 1 cm thickness and appropriately averaged over similar spectra for multiple randomly oriented crystals (Fig. 2d). The molar absorption coefficient $I(\nu)$ of Paterson (1982) with an 'orientation factor' of 0·5 was used to calculate the concentration of water, which was then multiplied by 3·5 following the calibration of Bell *et al.* (2003).

The spectrum of the as-received specimen can be resolved into two components, a sharp peak at 3690 cm^{-1}, reflecting the presence of hydrous phases, and a broader band around 3200–3600 cm^{-1}. The sharp peak was eliminated and the broad-band absorption greatly diminished by firing under controlled atmosphere at 1200°C (Fig. 2a), consistent with breakdown of the hydrous phases and expulsion of most of the molecular water (Table 1).

Mechanical testing

The experimental conditions and specimen characteristics are presented in Table 1. The pre-fired specimens were wrapped in $Ni_{70}Fe_{30}$ foil and the oven-dried specimens were either wrapped in $Ni_{70}Fe_{30}$ foil or sealed within a welded Pt capsule for mechanical testing within an outer mild-steel jacket with torsional forced-oscillation methods (Jackson & Paterson, 1993; Jackson, 2000). At the outset of each experiment, the assembly was first annealed (for 45–100 h) at the highest temperature [1300°C for pre-fired and oven-dried Ni-Fe wrapped specimens and 1150°C for Pt-sealed specimen] and 200 MPa confining pressure. During this interval, forced-oscillation tests were repeatedly conducted to monitor time dependence in the mechanical behaviour associated with any microstructural evolution. After stabilization of the mechanical behaviour, mechanical data were collected during slow staged-cooling (1–2°C/min) from the annealing temperature to room temperature. The IR spectroscopy for the recovered oven-dried Ni–Fe wrapped specimen (1066) indicated that it retained no more water than the pre-fired specimen (1055; Table 1)—in contrast to previous experiments of shorter duration with similar assemblies (Chopra & Paterson, 1981). The alternative of a welded stainless steel capsule lined internally with sleeves of talc and Ni used in compressive tests by Mei & Kohlstedt (2000) was rejected as

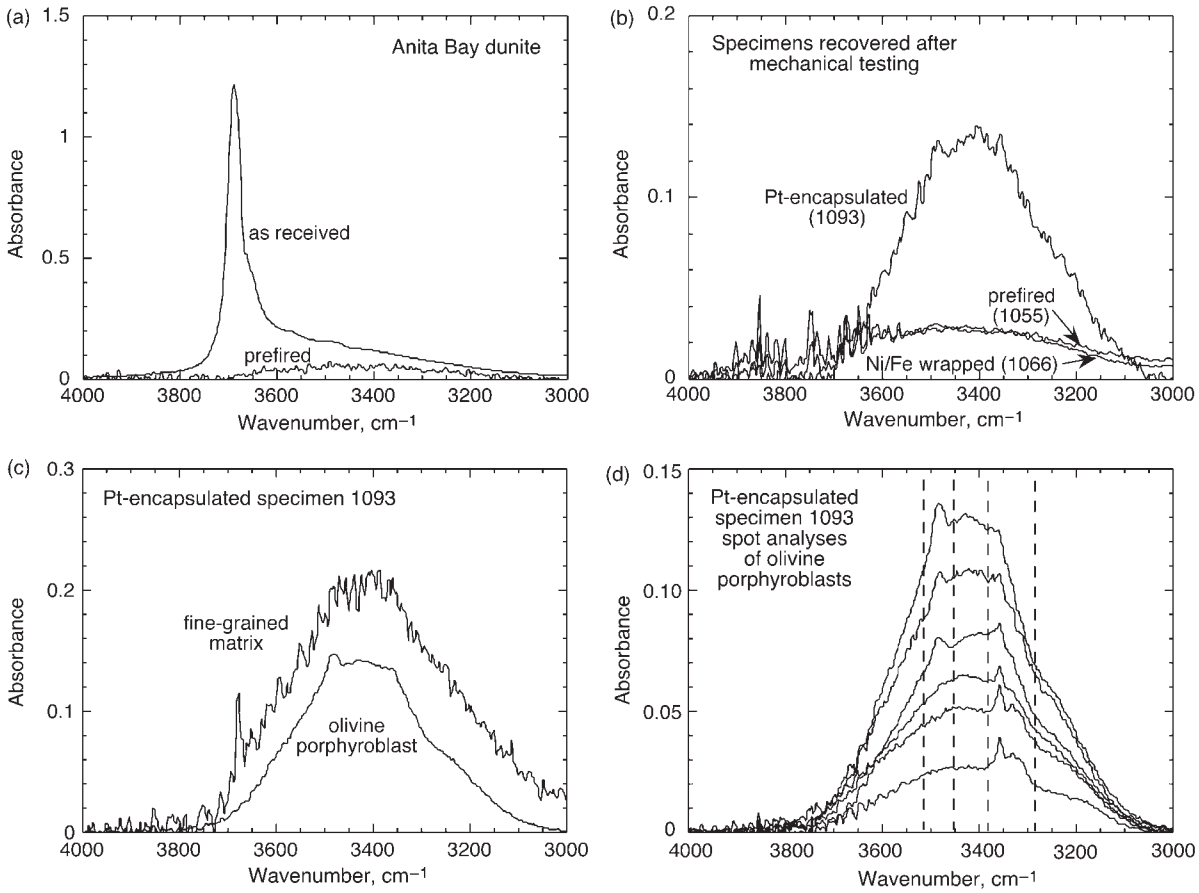

Fig. 2. Unpolarized Fourier transform IR (FTIR) spectra for dunite specimens, as-received and recovered following pre-firing and/or prolonged high-temperature mechanical testing [absorption coefficients plotted in (a)–(c) are normalized to 500 μm thickness]. (a) IR absorption spectra for the as-received and newly pre-fired bulk specimens; (b) IR absorption spectra for the oven-dried (1066) and pre-fired (1055) foil-wrapped bulk specimens and for the Pt-encapsulated bulk specimen (1093) recovered following high-temperature mechanical testing; (c) representative IR spectra (70 μm diameter spot analyses) for an olivine porphyroblast and the fine-grained matrix in Pt-encapsulated specimen (1093); (d) spectra for selected 70 μm diameter regions within randomly oriented olivine porphyroblasts in Pt-encapsulated specimen 1093 at a thickness of 460 μm; dashed lines highlight the regions occupied by the absorption peaks associated with structurally bound hydroxyl (see text for interpretation).

Table 1: Experimental conditions and characteristics of Anita Bay dunite specimens

Run no.:	As-received	1055	6570	1066	6573	1086	1093	6579
Prior heat treatment, foil/capsule		Pre-fired, Ni–Fe	Recovered from 1055	Untreated, Ni–Fe	Recovered from 1066	Pre-fired, Ni–Fe	Untreated, Pt	Untreated, Pt
T_{max} (°C)		1300	Re-equilibrated at 1300	1300	Re-equilibrated at 1300	1300	1150	1150
Recovery history		Stage-cooled	Quenched	Stage-cooled	Quenched	Stage-cooled	Stage-cooled	Quenched
Melt (fluid) fraction (vol. %)		0·01	0·02	0·1	0·1	0.05	0[2]*	0·1
Weight loss on ignition (%)	0·20						0·28	
Bulk [H_2O] (wt ppm)†	162	38		36		34	187	156

*Contains no detectable melt but 2% porosity.
†Based on the free-water absorption coefficient of Rossman (1988), excluding water in hydrous phases of as-received material.

impractical for quantitative torsional oscillation tests because of the difficulty of correcting the results for the unknown and potentially time-dependent complex modulus of the dehydrating talc sleeve. Instead, we conducted further measurements with the specimen enclosed within a welded Pt capsule of ~280 μm cylindrical wall thickness and 100 μm thick ends, to achieve H_2O-saturated conditions.

The data obtained from the forced-oscillation tests were processed to obtain the shear modulus G and strain-energy dissipation Q^{-1} vs period T_o for the interval 1–1000 s (Jackson *et al.*, 2004). In a significant refinement of established procedures, the calibration factors for the displacement transducers were corrected for drift during the long intervals (typically 5–9 h) of pre-programmed data acquisition. The torsional compliance of the specimen assembly was compared with that for a foil-free reference assembly containing an alumina control specimen. Combined G and Q^{-1} data for relatively high temperatures (800–1300°C) for each specimen were parameterized in an internally consistent manner with a phenomenological model based on a Burgers-type creep function (Faul & Jackson, 2005; Jackson, 2005) briefly described in Table 2 (first footnote). Owing to the low strain amplitudes (~10^{-5}) of torsional oscillation, the microstructures remained unchanged by mechanical testing.

RESULTS

Overview of shear modulus and dissipation data

The forced-oscillation data (both shear modulus G and dissipation Q^{-1} at high temperatures, T>1000°C for pre-fired and oven-dried, T>800°C for Pt-encapsulated

Table 2: Parameters of Burgers-type model fitted to the G and Q^{-1} data for the various specimens of Anita Bay dunite*

Run no.:	1055 Pre-fired (Ni–Fe) Background only 1000–1300°C	1066 Oven-dried (Ni–Fe) Background only 1000–1300°C	1086 Pre-fired (Ni–Fe) Background only 1000–1300°C	1093 Oven-dried, Pt-encapsulated Background only 800–1120°C†
J_U	1·78(2)E − 02	1·73(2)E − 02	1·41(1)E − 02	1·75(1)E − 02
$(\delta \ln J_U/\delta T)_R$	2·7(5)E − 04	5·9(6)E − 04	6·6(6)E − 04	4·2(5)E − 04
Δ	1·89	1·41	2·00	4·00
α	4·28(8)E − 01	2·73(7)E − 01	4·37(8)E − 01	2·54(8)E − 01
log τ_{LR}	−6·40E − 01	1·29E − 01	−5·00E − 01	−4·00E − 00
log τ_{HR}	6·33(8)	7·26(12)	6·79(8)	6·34(13)
log τ_{MR}	5·61(8)	6·85(12)	6·23(8)	4·34(13)
E	3·94(8)E + 05	5·09(13)E + 05	4·36(8)E + 05	4·76(13)E + 05
N	134	138	134	164
χ^2 (G)‡	24·8	38·2	37·1	112·2
χ^2 (Q^{-1})‡	111·3	74·2	57·6	71·3
χ^2 (total)	136·1	112·4	94·7	183·5

*The dependence of G and Q^{-1} upon oscillation period and temperature were fitted to the complex compliance expressed in terms of the Laplace transform of the generalized Burgers creep function:

$$J(t) = J_U \left\{ 1 + \delta \ln J_U(T) + \Delta \int_0^\infty D(\tau)[1 - \exp(-t/\tau)]d\tau + t/\tau_M \right\}$$

(Jackson, 2005). J_U is the unrelaxed compliance, which is the reciprocal of the unrelaxed shear modulus, $\tau_M = \eta J_U$ is the Maxwell relaxation time corresponding to viscosity η, and Δ is the relaxation strength associated with the distribution of anelastic relaxation times specified as $D(\tau) = \alpha\tau^{\alpha-1}/(\tau_H{}^\alpha - \tau_L{}^\alpha)$ for $\tau_L < \tau < \tau_H$ and zero elsewhere. The upper and lower limits to the distribution of anelastic relaxation times, respectively τ_H and τ_L, and the Maxwell relaxation time τ_M are each of the form $\tau = \tau_R \exp[(E/R)(1/T - 1/T_R)]$, where τ_R is the value of τ at the reference temperature T_R (here 950°C). $\delta \ln J_U(T) = (\delta \ln J_U/\delta T)(T - T_R)$ accounts for the temperature dependence of J_U including both anharmonic and relatively short-period viscoelastic effects (Jackson, 2005).
†Long-period data systematically excluded for $T \geq$ 1025°C (open symbols of Fig. 5).
‡Based on *a priori* errors: $\sigma(G)/G = 0{\cdot}03$ and $\sigma[\log_{10}(Q^{-1})] = 0{\cdot}05$.

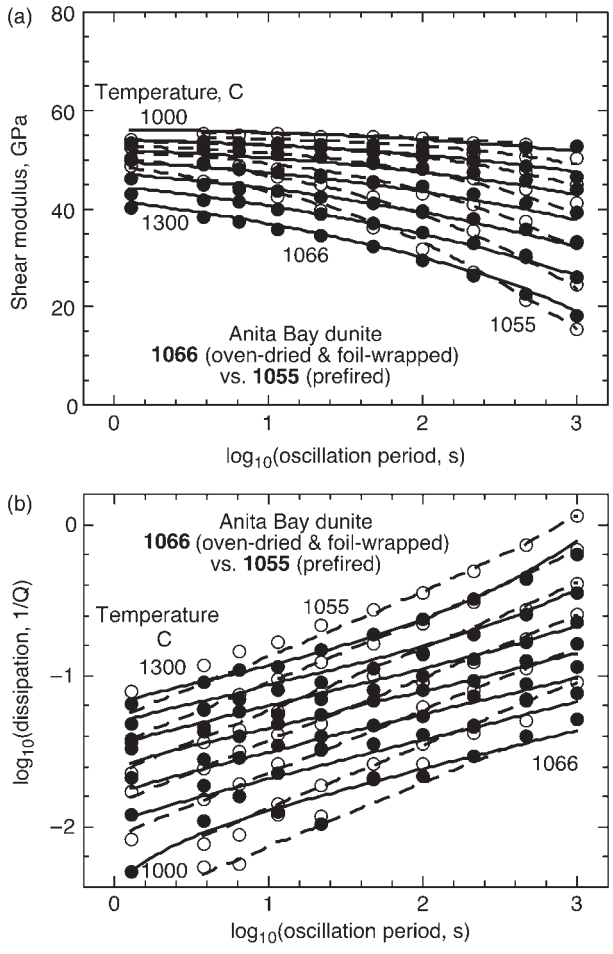

Fig. 3. Comparison of the results of forced-oscillation tests for pre-fired (1055, open symbols and dashed curves) and oven-dried specimens (1066, filled symbols, continuous curves). Data obtained at 50° intervals between 1300 and 1000°C are represented by the plotting symbols whereas the curves correspond to the extended Burgers model (Table 2) fitted simultaneously to all of the G and Q^{-1} data (with $\log_{10} Q^{-1} > -2{\cdot}4$) for $1000 < T < 1300$°C and $1 < T_o < 1000$ s.

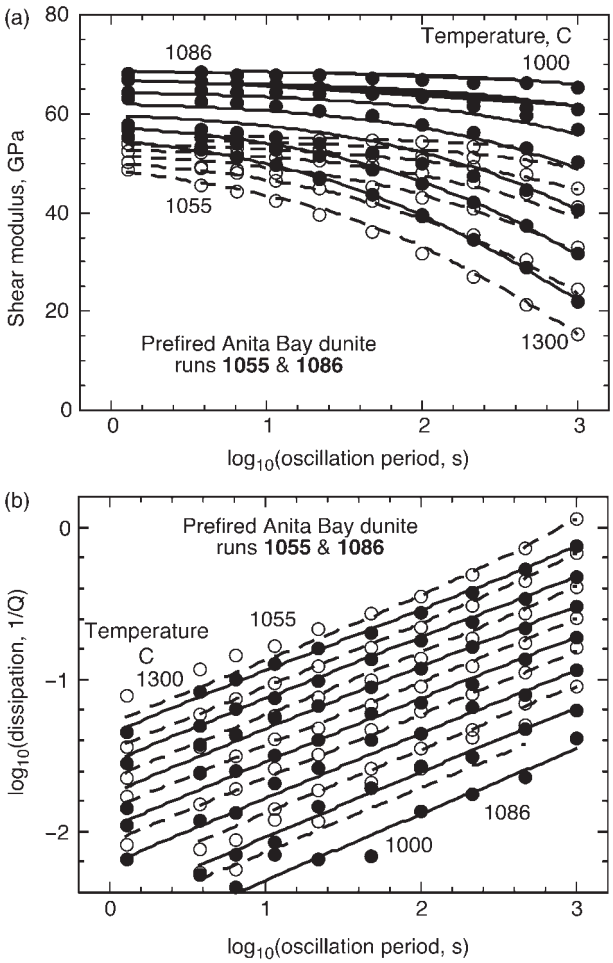

Fig. 4. Comparison of the results of forced-oscillation tests for the duplicate pre-fired specimens 1055 (open symbols and dashed curves) and 1086 (filled symbols and continuous curves). Otherwise the significance of the plotting symbols and curves is as for Fig. 3.

specimen) show strong viscoelastic behaviour and are generally well fitted by the Burgers model as illustrated in Figs 3–6. The parameters of the Burgers model for each of the four specimens are listed in Table 2. Monotonic variation of Q^{-1} with oscillation period for each specimen is observed, which is similar to that obtained in previous studies for 'melt-free' olivine aggregates (e.g. Jackson *et al.*, 2002), in spite of the presence in each specimen of a small silicate melt fraction, and in the Pt-encapsulated specimen, of ~2 vol. % of an aqueous fluid phase (see Microstructures section below). At lower temperatures, the specimen behaves nearly elastically, with relatively low levels of dissipation (<0·01) and no measurable dispersion. The usual mildly monotonic increase of shear modulus with decreasing temperature is disrupted at low temperatures (<600°C, not plotted) by thermal micro-cracking attributed to the relatively large grain-size and multi-phase character of the dunite material under conditions of relatively low confining pressure (200 MPa).

Although the Pt-encapsulated specimen was mechanically tested at a substantially lower maximum temperature (1150°C) than for the other specimens (1300°C), the magnitudes of the dissipation Q^{-1} for these different conditions are broadly comparable, indicating that the presence of H_2O has considerable influence on the mechanical behavior.

Comparison of G and Q^{-1} data for the Ni–Fe-wrapped oven-dried (1066) and pre-fired (1055 and 1086) specimens

As shown in Fig. 3, the pre-fired (1055) and oven-dried (1066) specimens display broadly similar levels of dissipation, but with a dependence on oscillation period T_o that

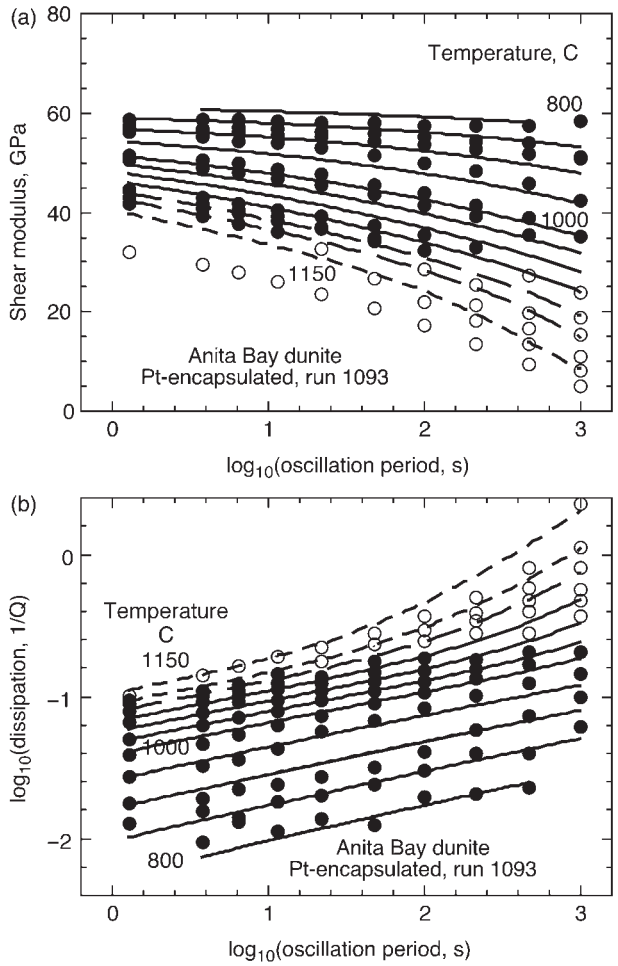

Fig. 5. Results of forced-oscillation tests on the Pt-encapsulated specimen (1093). Data were obtained at ~25° intervals between 1150 and 1000°C and at 50° intervals for 1000–800°C. Data indicated by the filled symbols were used to constrain the extended Burgers fit represented by continuous curves in the region where it is constrained by data and by dashed lines elsewhere. The open symbols represent data not used in constraining the model.

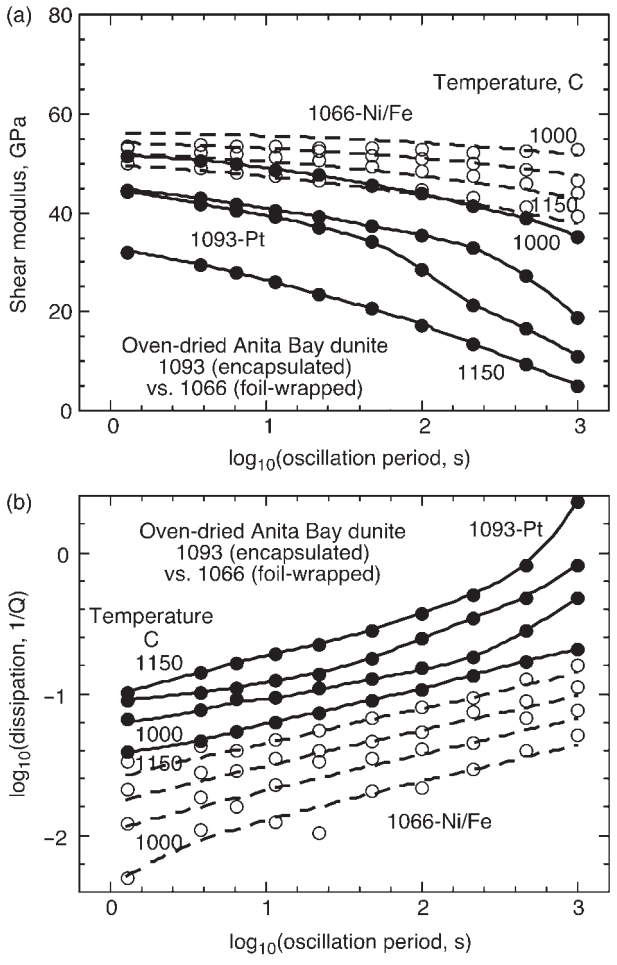

Fig. 6. Comparison of selected data, at 50° intervals between 1150 and 1000°C, for the oven-dried specimens 1066 (Ni–Fe-wrapped, open symbols and dashed curves) and 1093 (Pt-encapsulated, filled symbols and continuous curves).

is markedly stronger for the pre-fired specimen (1055) ($\partial \log Q^{-1}/\partial \log T_o \sim \alpha = 0{\cdot}43$ compared with $\alpha = 0{\cdot}27$ for the oven-dried specimen, Table 2). The systematically lower values of Q^{-1} at short periods for specimen 1055 are associated with a narrower spread of the values of the modulus at short period, which is reflected in a value ($2{\cdot}7 \times 10^{-4}\,K^{-1}$) of $\delta \ln J_U/\delta T$, the temperature sensitivity of the unrelaxed compliance (Table 2, first footnote), that is not much greater than the anharmonic value for Fo_{90} olivine ($2{\cdot}1 \times 10^{-4}\,K^{-1}$, Anderson & Isaak, 1995). This indicates that significant dissipation does not extend to relaxation times much shorter than 1 s even for temperatures as high as 1300°C. An experiment on another pre-fired specimen (run 1086) of Anita Bay dunite (Fig. 4), confirms the strong frequency dependence of Q^{-1} for the pre-fired material but with consistently somewhat lower Q^{-1} and significantly higher G for 1086 presumably reflecting the heterogeneity in the Anita Bay dunite boulder from which the specimens were cored.

Comparison of G and Q^{-1} data for the oven-dried specimens 1066 (Ni–Fe-wrapped) and 1093 (Pt-encapsulated)

For the Pt-encapsulated specimen (1093), a satisfactory fit to the Burgers model required exclusion of data pertaining to the highest temperatures and longest periods (e.g. 214–1000 s at 1075°C, 22–1000 s at 1120°C and 1–1000 s at 1150°C; Fig. 5). The excluded Q^{-1} data are in fact broadly compatible with the fit to the lower temperature data but this is not valid for G. Thus, there is a significant reduction in modulus at relatively long periods and temperatures >1000°C without any associated increase in Q^{-1}. The possibility that the modulus deficit reflects the

high pore pressure of H_2O will be addressed in the following section.

Q^{-1} is consistently higher for the Pt-sealed specimen 1093 than for the Ni–Fe-wrapped specimen 1066 by ~0·5 log unit, but the frequency dependences are broadly consistent (with $\alpha \sim 0{\cdot}26$; Fig. 6). The offset is essentially independent of temperature. The shear modulus is substantially lower for 1093 than for 1066 in the regime where the extended Burgers fit applies. The systematically lower modulus and greater dissipation for the former specimen suggest that the presence of water might play an important role in the mechanical behaviour.

Characteristics and microstructures of recovered specimens

Microstructures

Representative microstructures for three types of recovered specimen are shown in Figs 1, 7 and 8. The melt fractions for the oven-dried and pre-fired specimens (Table 1) were estimated via light microscopy and scanning electron microscopy (SEM). Recovered specimens re-equilibrated and quenched from 1300°C at 300 MPa, expected to preserve the maximum melt fraction relevant to experimental conditions, show generally very small melt fractions averaging <0·1%. Melt is distributed heterogeneously and is concentrated in areas where amphibole or chlorite was present or in adjacent olivine-rich regions of 100 μm grain size. Those hydrous phases have decomposed into olivine + orthopyroxene + melt ± clinopyroxene ± spinel. Melt fractions of up to 10 vol. % occur locally in those areas. Large gradients in melt fraction, particularly in pre-fired specimens, mean that melt fraction can drop to zero within as little as 50 μm distance from those former hydrous phases. On the sample scale, large areas with no melt present exist. In different parts of each sample, different melting paths are taken, in effective isolation, for different hydrous impurities. Consequently, the composition of glass formed by melt solidification is highly variable: for example, compositions in the pre-fired specimen (1055) show ranges of 53–58 wt % for SiO_2, 14–21 wt % Al_2O_3 and are very potassic, with ~3 wt % K_2O (Table 3). In the specimens that have been stage-cooled for attenuation measurements, the melts formed at high temperatures would have had the opportunity to partially crystallize.

For the oven-dried Ni–Fe-wrapped specimen (1066) subject to progressive dehydration during the course of the mechanical testing, the initial melting presumably occurred in the presence of an interconnected aqueous pore fluid with $P_f \sim P_c$ (see Discussion) explaining the more uniform glass composition (especially SiO_2, Al_2O_3, CaO, Na_2O and K_2O; Table 3), than for 1055. The much higher melt fraction in the recovered material than for

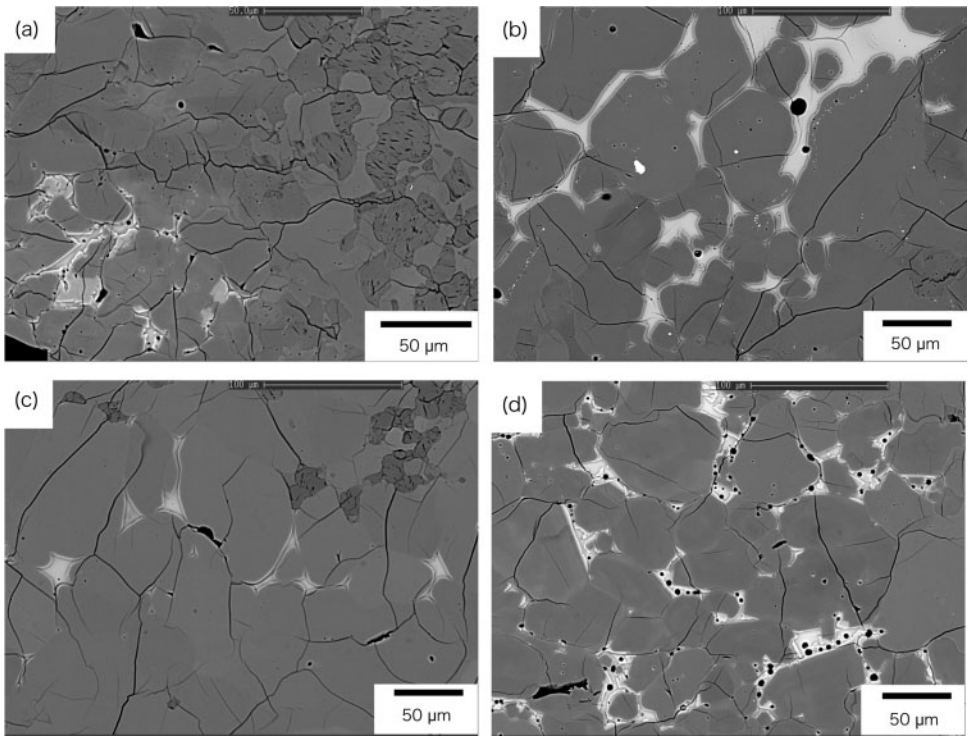

Fig. 7. Representative scanning electron micrographs of microstructures of the recovered specimens re-equilibrated at 1300°C: (a), (b) for the pre-fired (6570) and (c), (d) for the oven-dried Ni-Fe-wrapped specimens (6573) (gray, olivine; dark gray, orthopyroxene; white, melt and clinopyroxene). Large gradients of melt concentration are clearly observed in each specimen.

1055 presumably reflects a higher proportion of the non-olivine phases in that core.

For the specimen (6579) quenched from 1150°C under Pt-encapsulated conditions, the melt retained (~0·1 vol. %) is relatively homogeneously distributed and also reasonably uniform in chemical composition except for MgO and FeO, but is distinctively higher in SiO_2 and lower in Na_2O than the other melts. The melt pockets contain euhedral–subhedral orthopyroxene and subordinate clinopyroxene along with residual silicate melt. The melt composition (Table 3) is lower in Na_2O but otherwise closely comparable with the nano-crystalline plagioclase previously reported in melt-bearing olivines recovered from staged cooling (Faul *et al.*, 2004).

In contrast, the Pt-encapsulated specimen 1093 recovered after staged cooling contains no detectable melt even at sites where the microstructure and mineral assemblage point to the prior existence of hydrous-phase grains. However, the average 2 vol. % porosity is distributed heterogeneously throughout the specimen with fractions locally up to 30% over regions of 300 μm^2 at prior hydrous-grain sites. Because 6579, quenched from 1150°C, showed a small amount of melt (~0·1 vol. %), it seems reasonable to assume that 1093 similarly contained a small amount of melt at the highest temperature. Apparently this melt had almost completely crystallized during staged cooling in the presence of 2 vol. % of an aqueous phase. Many olivine–olivine grain boundaries

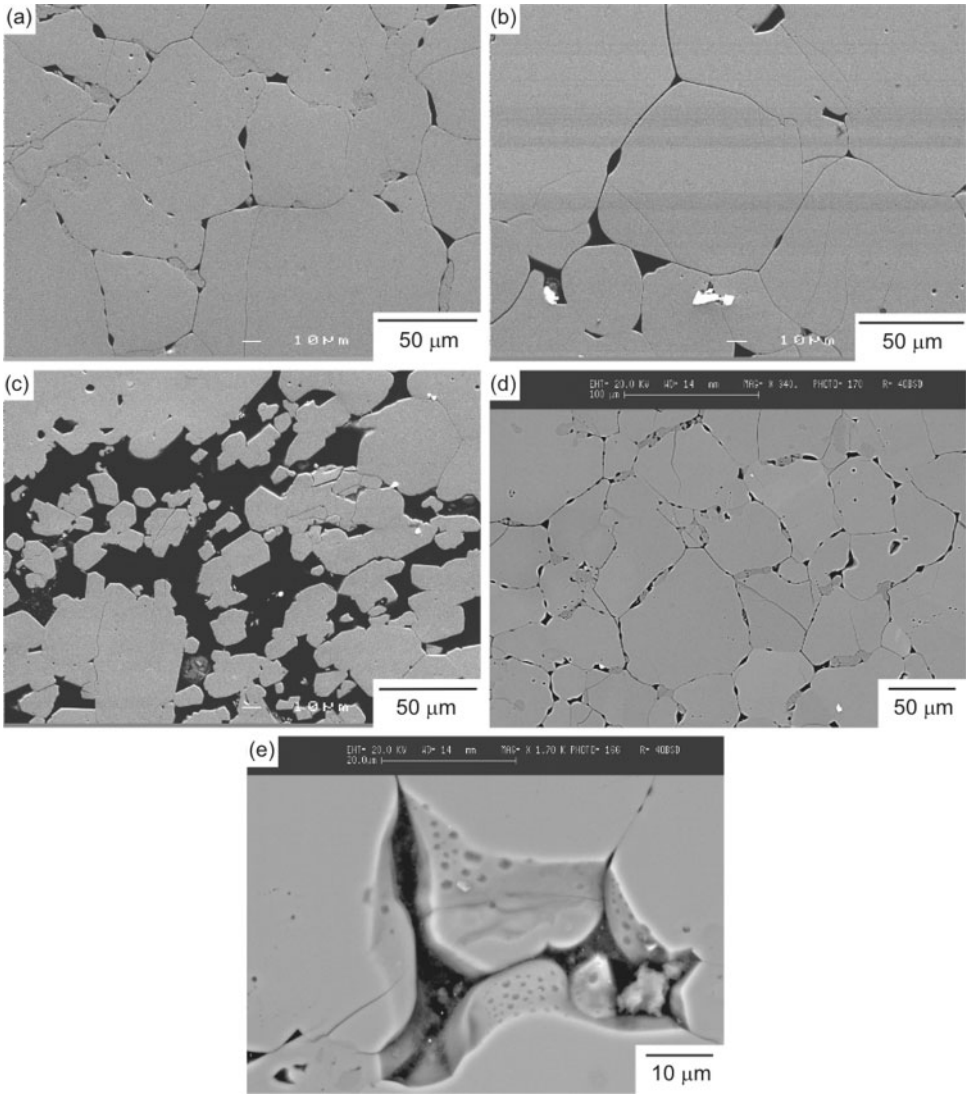

Fig. 8. Scanning electron micrographs showing the ~2 vol. % porosity in Pt-encapsulated specimen 1093 created by the dehydration of the secondary hydrous phases, and modified to some degree by complete progressive crystallization (during staged cooling from 1150°C) of ~0·1 vol. % silicate melt. In panels (a)–(d), the epoxy-filled pores on the polished surface yield few back-scattered electrons and appear dark. In (e), plucking of a grain during polishing created a cavity whose walls display arrays of isolated pores on grain-boundary surfaces.

Table 3: Chemical compositions of glasses (wt % oxides)

Run no.:	1055	1066	6579
	Pre-fired (Ni–Fe)	untreated (Ni–Fe)	Pt-encapsulated
T_{max}:	1300°C	1300°C	1150°C
	staged cooling	staged cooling	quenched
SiO_2	53–58	48–51	58–60
Al_2O_3	14–21	22–23	15–17
MgO	2·0–9·0	4·3–7·7	0·9–6·2
CaO	2·0–6·0	8·9–10	5·7–6·3
FeO	1·2–1·4	1·0–2·6	0·5–1·6
Na_2O	2·5–4·1	2·3–3·3	0·8–1·1
K_2O	2·8–3·3	0·4–0·6	0·5–0·7

contain micropore arrays, as well as larger lens-shaped pores with apparent dihedral angles of 30–50°. Olivine and orthopyroxene grains bordering the largest pore structures at grain junctions are conspicuously faceted. The pore volume has been partially redistributed into the olivine-dominant 100 μm grain-size regions, where the majority of triple junctions are occupied (pore volumes of 0·5–1·5%) indicating considerable connectivity of the pore fluids (Fig. 8). Original olivine grains have undergone grain growth in parts of these regions, and grain boundaries have become curved to straight (Fig. 1). The multitude of pore arrays and lenses, and the presence of many open grain boundaries are consistent with high and distributed fluid pressure and pervasive hydrofracturing.

Grain shape change and grain growth in the olivine-dominant regions were also clear in the oven-dried and Ni–Fe-wrapped specimen 1066 (Fig. 1), whereas the grain-boundary shapes in pre-fired specimen 1055 are indistinguishable from those of the starting material. It thus seems reasonable to speculate that grain-boundary mobility is positively correlated with the bulk OH content.

Water in the recovered specimens

The bulk molecular H_2O contents for the recovered specimens inferred from the IR absorption, as described above, are 34–38 wt ppm for pre-fired (1055 and 1086) and oven-dried Ni–Fe-wrapped specimens (1066) and 156–187 wt ppm for Pt-encapsulated specimens 6579 and 1093 (Table 1). The spot analyses of 1093 with 70 μm aperture reveal significant variability in $[H_2O]$ within and amongst the (randomly oriented) olivine porphyroblasts (Fig. 2d). $[H_2O]$ is systematically somewhat higher in matrix regions, implying that H_2O is preferentially accommodated in grain boundaries and in any small amount of glass (Fig. 2c).

Within the olivine porphyroblasts of 1093, broad-band absorption diagnostic of molecular water mainly in fluid inclusions is similarly dominant, at a level of ~20–80% of the absorbance for the bulk specimen (Fig. 2c). The superimposed sharp absorption peaks at 3353 and 3325 cm^{-1} are attributed to hydroxyl associated with the trivalent cations Fe^{3+} and Cr^{3+}, respectively, whereas the other prominent peak (at 3478 cm^{-1}) may reflect hydroxyl related to Si vacancies and/or Ti^{4+}-related defects (Berry *et al.*, 2005, 2007; Grant *et al.*, 2007; Walker *et al.*, 2007). Such sharp peaks (Fig. 2d) provide evidence of structurally bound hydroxyl at concentrations of 2–3 wt ppm H_2O. Evidence of newly crystallized hydrous phases, in the form of a sharp absorption peak at 3690 cm^{-1}, was also found in both bulk and matrix analyses (Fig. 2c). The weight loss on ignition of the recovered specimen (1093) was 0·28 wt % (Table 1), indicating that most of the volatiles initially contained in the specimen were retained in the Pt-capsule following sustained high-T mechanical testing.

DISCUSSION

Solid-state viscoelastic relaxation in dry dunite

The results of the present study that are most closely comparable with previous seismic-frequency data are for the oven-dried Ni–Fe-wrapped specimen 1066, recovered essentially dry. A useful comparison can be made with the Andrade–Gaussian pseudo-period model for Q^{-1} for a suite of synthetic melt-bearing olivine polycrystals (Jackson *et al.*, 2004, table 4). For comparison with the data from the present study for specimen 1066, this model has been evaluated at 100 μm grain size and at the representative melt fractions of 0·01 and 0·1 vol. %. A good match to the data for 1066 is obtained for $\phi = 0{\cdot}01\%$ (Fig. 9a). However, for $\phi = 0{\cdot}1\%$, the estimated melt fraction for specimen 1066 (Table 1), the model deviates systematically from the data at short periods where a subtle Q^{-1} plateau at temperatures of 1150–1250°C predicted by the model is not strongly expressed in the data (Fig. 9b). Thus there is no compelling evidence for a melt-related dissipation peak despite the fact that the olivine grain edges are perhaps sufficiently commonly rounded at grain-edge triple junctions (Fig. 7c) to facilitate elastically accommodated grain-boundary sliding as envisaged by Faul *et al.* (2004). However, the milder dependence of Q^{-1} upon oscillation period for the oven-dried Ni–Fe-wrapped specimen 1066 might in fact mask the presence of a dissipation peak of low amplitude associated with a silicate melt fraction somewhat greater and more uniformly distributed than for the pre-fired specimens.

Despite the microstructural complexities of Anita Bay dunite, the Andrade–Gaussian pseudo-period model of simple synthetic melt-bearing olivine (Jackson *et al.*, 2004)

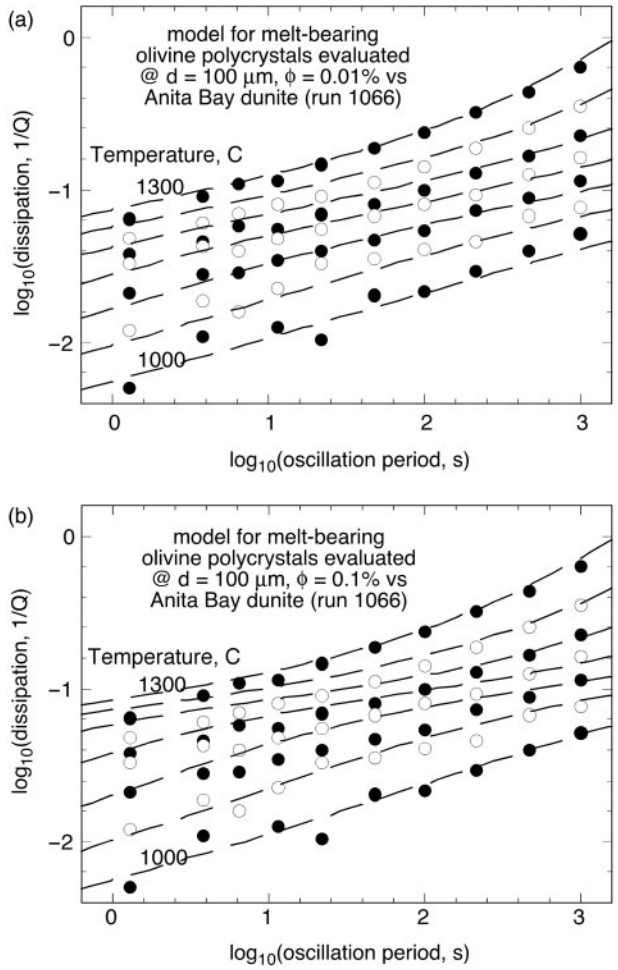

Fig. 9. Comparison of data (filled and open symbols for alternate temperatures between 1300 and 1000°C in intervals of 50°C) for oven-dried Ni–Fe-wrapped Anita Bay dunite specimen 1066 with the results of a previous study. (a) Comparison with an *a priori* model (dashed lines) for melt-bearing olivine polycrystals (Faul *et al.*, 2004) evaluated for a mean grain size of 100 μm and melt fraction $\phi = 0{\cdot}01\%$. (b) As for (a) but with $\phi = 0{\cdot}1\%$.

provides a reasonable approximation to the data for the natural dunite specimen 1066. This demonstrates that Anita Bay dunite can be usefully compared with simpler polycrystalline mantle rocks and that Anita Bay dunite can be used as a first-order proxy for mantle material in examination of the influence of water on seismic wave attenuation.

H_2O in the Pt-encapsulated specimen 1093

The results obtained for the Pt-encapsulated specimen (1093) display consistently lower shear modulus and higher dissipation than the foil-wrapped specimen 1066. To interpret this contrast in seismic properties, we first estimate the pore fluid pressure using the equation of state for pure H_2O given by Holland & Powell (1991, Fig. 2a). The volume ϕ and mass m_f fractions of the H_2O pore fluid are related by

$$\phi = [1 + (\rho_f/\rho_r)(1/m_f - 1)]^{-1}$$

where ρ_r and ρ_f are the densities of the rock matrix and fluid, respectively.

For $m_f = 0{\cdot}0028$ (for 1093, Table 1) and $\rho_r = 3{\cdot}3$ g/cm^3 and pore fluid pressure P_f of 200 MPa (equal to confining pressure P_c) ϕ is predicted to decrease linearly with temperature from 3·1% at 1150°C to 2·0% at 750°C—compared with our estimate of 2% porosity in the recovered specimen. At the highest temperatures of runs 1093 and 6579, the condition $P_f = P_c$ is thus expected to be realized. Any tendency for P_f to exceed P_c will be countered by swelling of the Pt capsule and enclosing steel jacket to increase the volume available for the pore fluid. On cooling, restoration of a significant differential pressure $P_d = P_c - P_f$ (sometimes called effective pressure) is expected for temperatures <750°C.

Considering the low initial porosity in the as-received dunite, the 2 vol. % porosity must have been created by dehydration accompanied by the development of a small silicate melt fraction, leading to high pore-fluid pressure and pervasive grain-boundary hydrofracturing. This microstructural evidence, along with the IR evidence of molecular water in fluid inclusions within the olivine porphyroblasts and the substantial weight loss of 0·28% on oven drying of the recovered specimen (Table 1), suggests that the specimen remained H_2O-saturated throughout the experiment (see Grant *et al.*, 2007). In these circumstances, the available H_2O would have been partitioned among a substantial volume fraction (~2%) of an aqueous fluid phase, a subordinate amount (~0·1% at the maximum temperature) of an immiscible silicate melt phase (e.g. Hirschmann *et al.*, 2005) subject to essentially complete progressive crystallization during staged cooling, and hydroxyl chemically bound in the crystal structure of the nominally anhydrous minerals.

Using the recent results of Zhao *et al.* (2004), we estimate the equilibrium solubility in the olivine of specimen 1093 to be 26 wt ppm H_2O at $P_c = P_f = 200$ MPa and 1150°C, for the relatively oxidizing conditions expected to prevail within the Pt capsule (Grant *et al.*, 2007). However, Mackwell & Kohlstedt (1990) reported re-equilibration of dissolved water on timescales of hours in millimetre-sized crystals during cooling to ~1000°C, suggesting that equilibrium in this study would have been maintained to lower temperatures of perhaps ~800°C during staged cooling involving 25°C steps and 6–10 h at each stage. This scenario is consistent with more recent data concerning H diffusivity reviewed by Ingrin & Blanchard (2006). At 800°C, a substantially lower solubility of about 8 wt ppm H_2O is expected (Zhao *et al.*, 2004). This estimate is to be compared with the concentrations of 2–3 wt ppm

H_2O for the olivine porphyroblasts in the Pt-encapsulated specimen from the sharp IR absorption peaks. Significant variability amongst the various porphyroblasts (Fig. 2d) probably reflects a combination of two factors: variation of absorbance with lattice orientation, and diffusion profiles associated with incomplete re-equilibration to lower [H_2O] during staged cooling (see Peslier & Luhr, 2006). The observed concentration of structurally bound hydroxyl in the olivine porphyroblasts of the Pt-encapsulated specimen, along with the presence of fluid inclusions, is therefore broadly consistent with expectations based on equilibrium partitioning with the pore fluid during staged cooling.

Water-enhanced solid-state viscoelastic relaxation

The Pt-encapsulated specimen 1093 has a similarly low value of α [0·25(1)] to 1066 (recovered essentially dry following *in situ* dehydration) but generally much higher Q^{-1} and lower G (Fig. 6). A modulus deficit, essentially independent of oscillation period, is attributed to the direct influence of the fluid phase as discussed in the next section. However, the water-saturated conditions maintained in specimen 1093 are also expected to promote solid-state viscoelastic relaxation—through a combination of grain-boundary and intragranular mechanisms. Increased grain-boundary mobility has already been inferred microstructurally. The effective grain-boundary viscosity η should be markedly reduced by the presence of the aqueous fluid phase, so that the characteristic timescale (is proportional to η) for relaxation associated with grain-boundary sliding might be significantly less than for essentially anhydrous conditions (e.g. for specimen 1066). The mild period dependence of Q^{-1} would then be explained as for 1066 by the superposition upon the dissipation background of a broad peak, having its impact at lower temperatures than for 1066 because of the influence of water in reducing the grain-boundary viscosity. The elevated water fugacity may also enhance intragranular viscoelastic relaxation by increasing the mobility of dislocations as suggested by Karato (2003).

The direct influence of the fluid phase

Both wetted grain boundaries and their tendency to evolve into arrays of isolated grain-boundary pores are evident in the Pt-encapsulated (1093) specimen (Fig. 8). However, the presence of pores at most olivine triple junctions indicates the preservation of high fluid connectivity. Presumably the hydrofracturing and high P_f created and maintained a high degree of boundary wetting at the highest temperatures. During subsequent staged cooling, P_f eventually became significantly less than P_c and the arrays of isolated grain-boundary pores began to form. In specimen 1093, the small silicate melt fraction evidently crystallized very effectively, and presumably early, during the staged cooling from 1150°C. In this scenario, it is the ~2 vol. % aqueous fluid phase, present throughout staged cooling but with progressively lower P_f, that is relevant to the observed viscoelastic relaxation.

It is widely recognized that elastic moduli and wave speeds will be influenced by the presence of a bulk pore fluid to a degree determined mainly by the properties of the porous or cracked rock matrix and the saturating fluid, notably the volume fraction ϕ of pore fluid, the aspect ratio of the fluid-filled 'inclusions' (defined as minimum/maximum dimension), and the bulk modulus of the fluid. The effective elastic properties are also predicted to vary with the timescale or frequency of the measurement. For the saturated isolated regime, probed at the MHz frequencies of ultrasonic techniques, experimentally determined elastic properties can be related to those of the dense matrix via the 'soft-fluid' saturation theory of O'Connell & Budiansky (1974). Ultrasonic methods have been used by Kono *et al.* (2007) to measure the reduction of compressional wave speed (V_P) resulting from the *in situ* dehydration of hydrous minerals in altered ultramafic rocks of low initial porosity encapsulated, like those of the present study, within welded metal containers. Observed reductions in V_P, reaching only 15% for $\phi = 0{\cdot}12$ at 1 GPa and 1000°C and interpreted as representative of the saturated isolated regime, suggest an average aspect ratio of ~0·15 indicative of sub-equant fluid inclusions rather than extensively wetted grain boundaries with aspect ratios <0·01.

For conditions representative of the present study of specimen 1093 ($\phi = 0{\cdot}02$ and water saturation with $P_c = P_f = 200$ MPa at 1150°C), and the average aspect ratio of 0·15 inferred from the preceding analysis, a shear modulus reduction of ~5% would be predicted within the saturated isolated regime. A further ~2% shear modulus relaxation would be expected under these conditions from local fluid flow [O'Connell & Budiansky, 1977, equation (25)] yielding an essentially frequency-independent modulus deficit of perhaps 7% for the saturated isobaric regime presumably probed by the present low-frequency forced-oscillation measurements.

At the highest temperatures of the present study, the pressurized fluid phase may exert additional influence by compromising the mechanical coupling between torsion rods and specimen that depends upon maintenance of significant differential pressure P_d (Jackson *et al.*, 1984). Low P_d provides a plausible explanation for the anomalous reduction of modulus without associated dissipation evident at progressively longer periods for temperatures above 1000°C.

The direct influence of the fluid phase on the measured modulus is expected to diminish during staged cooling on account of the previously mentioned microstructural changes. As grain boundaries that were at least transiently

wetted at $P_f \sim P_c$ evolve to form the arrays of isolated grain-boundary pores and the connected grain-edge tubules at lower T and P_f, the average aspect ratio of the fluid inclusions will increase substantially, resulting in a progressively smaller modulus deficit.

In summary, these first forced-oscillation data provide compelling evidence of markedly lower shear moduli and higher attenuation under water-saturated conditions. These effects are attributable in part to the presence of a bulk pore fluid and partly to the enhancement of solid-state relaxation processes by the high water fugacity. However, the heterogeneity and microstructural complexity of the Anita Bay dunite tested in this exploratory study preclude a definitive quantitative interpretation. It is intended that a further study on the role of water on seismic wave attenuation will use simpler synthetic polycrystalline olivine specimens. Such a study will provide more conclusive answers concerning the effect of water on seismic wave attenuation in the upper mantle.

GEOPHYSICAL IMPLICATIONS

As discussed in the previous section, the homogeneous distribution of fluids along grain boundaries, presumably resulting from hydrofracturing, is consistent with our semi-quantitative estimate of $P_f \sim P_c$ at high temperature. Broadly analogous conditions may be realized, at least transiently, during dehydration of subducting oceanic lithosphere, where pore pressures comparable with the prevailing lithostatic pressure might induce hydrofracturing, thereby facilitating fluid transport into the overlying mantle wedge triggering partial melting (Davies, 1999). The development and persistence of such conditions of high pore-fluid pressure will depend strongly on the grain-scale permeability, which is a function of the instantaneous wetting behaviour and the temporal evolution of the fluid–solid microstructure (e.g. Faul, 1997). Increasing pressure with depth in the upper mantle increases the silica content of the aqueous fluid resulting in lower dihedral angles, connectivity of the fluid phase distributed in grain-edge tubules, and hence higher permeability (e.g. Mibe *et al.*, 1998). The presence of a few per cent of a fluid phase thus accommodated mainly in grain-edge tubules would have limited impact upon the seismic wave speeds. However, the complete wetting of grain boundaries, inferred for the highest temperatures of the present study and recently reported by Yoshino *et al.* (2007) for pressures corresponding to the deepest part of the upper mantle, results in much larger reductions in wave speeds that are likely to be seismologically observable. Thus the reduced wave speeds and pronounced dissipation observed in the fluid-pressurized specimens of the present study and that of Kono *et al.* (2007) may be relevant particularly to the deepest zones of low velocity and high attenuation in mantle-wedge environments (e.g. Zhao *et al.*, 1992; Takanami *et al.*, 2000; Nakajima & Hasegawa, 2003). However, the very different timescales for grain-scale hydrofracturing, textural re-equilibration and fluid migration in the laboratory and subduction-zone settings, along with the markedly different fluid compositions, preclude any immediate quantitative seismological application of these experimental data.

SUMMARY

An exploratory study of the role of water in upper-mantle seismic-wave attenuation and dispersion has been undertaken on a natural dunite, of 100 μm average olivine grain size, containing ~0·3 wt % H_2O mainly in accessory hydrous silicate minerals. Cylindrical samples, either oven-dried or thoroughly dehydrated by pre-firing at 1200°C under controlled atmosphere, and either wrapped in Ni–Fe foil or sealed within a welded Pt capsule, have been tested in torsional forced oscillation at seismic periods of 1–1000 s and low strain amplitudes, under conditions of simultaneous high pressure (200 MPa) and temperature (to 1300°C).

Both oven-dried and pre-fired specimens, wrapped in Ni–Fe foil in the standard vented experimental assembly, were recovered after staged cooling following annealing for tens of hours at 1300°C and 200 MPa, containing no more than 40 wt ppm bulk molecular H_2O. On the other hand, Pt encapsulation of dunite allows retention of essentially the entire inventory of water, including 150 wt ppm bulk molecular water trapped as fluid inclusions in the recovered specimens, for the duration of similar experiments at peak temperatures of 1150°C. *In situ* dehydration of the hydrous minerals liberates water at a pore pressure P_f locally and transiently greater than the confining pressure, resulting in pervasive hydrofracturing and redistribution of the dominant aqueous fluid and coexisting minor silicate melt phases. During staged cooling from 1150°C the ~2 vol. % porosity thus created is occupied mainly by the aqueous pore fluid. The decrease of P_f with decreasing temperature leads eventually to the restoration of a significantly positive differential pressure $P_d = P_c - P_f$ and a consequent transition from grain-boundary wetting for $P_d \sim 0$ towards arrays of isolated grain-boundary pores for $P_d > 0$.

Each specimen displays intense viscoelastic relaxation at sufficiently high temperatures; both pronounced dissipation Q^{-1} and associated inverse dependence of the shear modulus upon oscillation period are measured. The behaviour is of the 'high-temperature background' type, whereby Q^{-1} varies monotonically with period and temperature without any well-resolved dissipation peak. For each of the pre-fired specimens, the absence of a melt-related dissipation peak is attributed to the highly localized distribution of a small melt fraction ($\leq$0·05 vol. %); the bulk of the specimen is simply melt-free. For the Ni–Fe-wrapped oven-dried specimen (1066), the somewhat more abundant

melt (0·1 vol. %) is more uniformly distributed on account of the hydrofracturing associated with transiently high P_f early in the experiment. A poorly resolved broad melt-related peak of low amplitude superimposed on the background dissipation may explain the milder period dependence of Q^{-1} for this specimen.

Where ~2 vol. % of an aqueous fluid phase is retained (in the Pt-encapsulated specimen) the lowest shear moduli and highest levels of attenuation were measured. The mild period dependence of Q^{-1}, like that for 1066, may be attributable to the superposition on the background of a poorly resolved dissipation peak associated with grain-boundary sliding. The higher dissipation and lower modulus for a given temperature (Fig. 6) than for specimen 1066 may reflect both water-enhanced solid-state relaxation (grain-boundary and intragranular mechanisms) and the direct influence of the fluid phase. The anomalously low moduli measured at the highest temperatures are attributed to conditions of low differential pressure resulting in extensive wetting of grain boundaries by aqueous fluid and compromised mechanical coupling between the specimen and torsion rods. It has been shown in this exploratory study that water may have a significant effect on seismic wave attenuation in mantle material, thereby giving incentive for more detailed studies.

ACKNOWLEDGEMENTS

The expert assistance of Harri Kokkonen and Craig Saint in the preparation of specimens and experimental assemblies, and in microstructural characterization, is gratefully acknowledged. We thank David Green for his consistent support of our work on seismic wave attenuation in upper-mantle materials and for his valuable guidance on petrological matters. Detailed reviews by S. Karato and anonymous reviewers of earlier versions of the manuscript are greatly appreciated.

REFERENCES

Anderson, D. L. & Hart, R. S. (1978). *Q* of the Earth. *Journal of Geophysical Research* **83**, 5869–5882.

Anderson, D. L. & Isaak, D. G. (1995). Elastic constants of mantle minerals at high temperature. In: Ahrens, T. J. (ed.) *Mineral Physics and Crystallography: A Handbook of Physical Constants, AGU Reference Shelf, Vol. 2*. Washington, DC: American Geophysical Union, pp. 64–97.

Bell, D. R., Rossman, G. R., Maldener, J., Endisch, D. & Rauch, F. (2003). Hydroxide in olivine: A quantitative determination of the absolute amount and calibration of the IR spectrum. *Journal of Geophysical Research* **108**, doi:10.1029/2001JB000679.

Berry, A. J., Hermann, J., O'Neill, H. St. C. & Foran, G. J. (2005). Fingerprinting the water site in mantle olivine. *Geology* **33**, 869–872.

Berry, A. J., O'Neill, H. St. C., Hermann, J. & Scott, D. R. (2007). The infrared signature of water associated with trivalent cations in olivine. *Earth and Planetary Science Letters* **261**, 134–142.

Carter, N. L. & Avé Lallemant, H. G. (1970). High-temperature flow of dunite and peridotite. *Geological Society of America Bulletin* **81**, 2181–2202.

Chopra, P. N. & Paterson, M. S. (1981). The experimental deformation of dunite. *Tectonophysics* **78**, 453–473.

Chopra, P. N. & Paterson, M. S. (1984). The role of water in the deformation of dunite. *Journal of Geophysical Research* **89**, 7861–7876.

Cooper, R. F. (2002). Seismic wave attenuation: Energy dissipation in viscoelastic crystalline solids. In: Karato, S. & Wenk, H. (eds) *Plastic Deformation in Minerals and Rocks. Mineralogical Society of America, Reviews of Mineralogy and Geochemistry* **51**, 253–290.

Davies, J. H. (1999). The role of hydraulic fractures and intermediate depth earthquakes in generating subduction-zone magmatism. *Nature* **398**, 142–145.

Faul, U. H. (1997). Permeability of partially molten upper mantle rocks from experiments and percolation theory. *Journal of Geophysical Research* **102**, 10299–10311.

Faul, U. H. & Jackson, I. (2005). The seismological signature of temperature and grain size variations in the upper mantle. *Earth and Planetary Science Letters* **234**, 119–134.

Faul, U. H. & Jackson, I. (2007). Diffusion creep of dry, melt-free olivine. *Journal of Geophysical Research* **112**, B04204, doi:10.1029/2006JB004586.

Faul, U. H., Fitz Gerald, J. D. & Jackson, I. (2004). Shear-wave attenuation and dispersion in melt-bearing olivine polycrystals II. Microstructural interpretation and seismological implications. *Journal of Geophysical Research* **109**, B06202, doi:10.1029/2003JB002407.

Grant, K., Brooker, R. A., Kohn, S. C. & Wood, B. J. (2007). The effect of oxygen fugacity on hydroxyl concentrations and speciation in olivine: Implications for water solubility in the upper mantle. *Earth and Planetary Science Letters* **261**, 217–229.

Gribb, T. T. & Cooper, R. F. (1998). Low-frequency shear attenuation in polycrystalline olivine: grain-boundary diffusion and the physical significance of the Andrade model for viscoelastic rheology. *Journal of Geophysical Research* **103**, 27267–27279.

Hirschmann, M. M., Aubaud, C. & Withers, A. C. (2005). Storage capacity of H_2O in nominally anhydrous minerals in the upper mantle. *Earth and Planetary Science Letters* **236**, 167–181.

Holland, T. J. B. & Powell, B. (1991). A Compensated-Redlich–Kwong (CORK) equation for volumes and fugacities of CO_2 and H_2O in the range 1 bar to 50 kbar and 100–1600°C. *Contributions to Mineralogy and Petrology* **160**, 170–182.

Ingrin, J. & Blanchard, M. (2006). Diffusion of hydrogen in minerals. In: Keppler, H. & Smyth, J. R. (eds) *Water in Nominally Anhydrous Minerals. Mineralogical Society of America, Reviews of Mineralogy and Geochemistry* **62**, 291–320.

Jackson, I. (2000). Laboratory measurement of seismic wave dispersion and attenuation: recent progress. In: Karato, S., Forte, A. M. & Liebermann, R. C. *et al.* (eds) *Earth's Deep Interior: Mineral Physics and Tomography from the Atomic to the Global Scale. Geophysical Monograph, American Geophysical Union* **117**, 265–289.

Jackson, I. (2005). Laboratory measurement of seismic wave dispersion and attenuation at high pressure and temperature. In: Chen, J., Wang, Y. & Duffy, T. S. *et al.* (eds) *Advances in High-pressure Technology for Geophysical Applications*. Amsterdam: Elsevier, pp. 95–115.

Jackson, I. (2007). Properties of rocks and minerals—physical origins of anelasticity and attenuation in rock. In: Schubert, G. (ed.) *Treatise on Geophysics, Volume 2*. Oxford: Elsevier, pp. 493–525.

Jackson, I. & Paterson, M. S. (1993). A high-pressure, high-temperature apparatus for studies of seismic wave dispersion and attenuation. *Pure and Applied Geophysics* **141**, 445–456.

Jackson, I., Paterson, M. S., Niesler, H. & Waterford, R. M. (1984). Rock anelasticity measurements at high pressure, low strain amplitude and seismic frequency. *Geophysical Research Letters* **11**, 1235–1238.

Jackson, I., Paterson, M. S. & Fitz Gerald, J. D. (1992). Seismic wave attenuation in Åheim dunite: an experimental study. *Geophysical Journal International* **108**, 517–534.

Jackson, I., Fitz Gerald, J. D., Faul, U. H. & Tan, B. H. (2002). Grain-size-sensitive seismic wave attenuation in polycrystalline olivine. *Journal of Geophysical Research* **107**, doi:10.1029/2001JB001225.

Jackson, I., Faul, U. H., Fitz Gerald, J. D. & Tan, B. H. (2004). Shear-wave attenuation and dispersion in melt-bearing olivine polycrystals I. Specimen fabrication and mechanical testing. *Journal of Geophysical Research* **109**, B06201, doi:10.1029/2003JB002409.

Kanamori, H. & Anderson, D. L. (1977). Importance of physical dispersion in surface wave and free oscillation problems: Review. *Review of Geophysics* **15**, 105–112.

Karato, S. (2003). Mapping water content in the upper mantle, In: Eiler, J. (ed.) *The Subduction Factory. Geophysical Monograph, American Geophysical Union* **138**, 135–152.

Karato, S. & Jung, H. (1998). Water, partial melting and the origin of the seismic low-velocity and high-attenuation zone in the upper mantle. *Earth and Planetary Science Letters* **153**, 193–207.

Karato, S. & Spetzler, H. A. (1990). Defect microdynamics in minerals and solid-state mechanism of seismic wave attenuation and velocity dispersion in the mantle. *Reviews of Geophysics* **28**, 399–421.

Karato, S. I., Paterson, M. S. & Fitz Gerald, J. D. (1986). Rheology of synthetic olivine aggregates: Influence of grain size and water. *Journal of Geophysical Research* **91**, 8151–8176.

Kohlstedt, D. L. (2006). The role of water in high-temperature rock deformation. In: Keppler, H. & Smyth, J. R. (eds) *Water in Nominally Anhydrous Minerals. Mineralogical Society of America, Reviews of Mineralogy and Geochemistry* **62**, 377–396.

Kono, Y., Ishikawa, M. & Arima, M. (2007). Effect of H_2O released by dehydration of serpentine and chlorite on compressional wave velocities of peridotites at 1 GPa and up to 1000°C. *Physics of the Earth and Planetary Interiors* **161**, 215–223.

Kovács, I., Hermann, J., O'Neill, H. St. C., Fitz Gerald, J. D., Sambridge, M. & Horvath, G. (2008). Quantitative absorbance spectroscopy with unpolarized light, Part II: Experimental evaluation and development of a protocol for quantitative analysis of mineral IR spectra. *American Mineralogist* (in press).

Mackwell, S. J. & Kohlstedt, D. L. (1990). Diffusion of hydrogen in olivine—implications for water in the mantle. *Journal of Geophysical Research* **95**, 5079–5088.

Mei, S. & Kohlstedt, D. L. (2000). Influence of water on plastic deformation of olivine aggregates 1. Diffusion creep regime. *Journal of Geophysical Research* **105**, 21457–21469.

Mibe, K., Fujii, T. & Yasuda, A. (1998). Connectivity of aqueous fluid in the Earth's upper mantle. *Geophysical Research Letters* **25**, 1233–1236.

Minster, J. B. & Anderson, D. L. (1981). A model of dislocation controlled rheology for the mantle. *Philosophical Transactions of the Royal Society of London, Series A* **299**, 319–356.

Muan, A. & Osborn, E. F. (1965). *Phase Equilibria among Oxides in Steelmaking*. Reading, MA: Addison Wesley.

Nakajima, J. & Hasegawa, A. (2003). Estimation of thermal structure in the mantle wedge of northeastern Japan from seismic attenuation data. *Geophysical Research Letters* **30**, 1760, doi:10.1029/2003GL017185.

Nowick, A. S. & Berry, B. S. (1972). *Anelastic Relaxation in Crystalline Solids*. New York: Academic Press.

O'Connell, R. J. & Budiansky, B. (1974). Seismic velocities in dry and saturated cracked solids. *Journal of Geophysical Research* **79**, 5412–5426.

O'Connell, R. J. & Budiansky, B. (1977). Viscoelastic properties of fluid-saturated cracked solids. *Journal of Geophysical Research* **82**, 5719–5735.

Paterson, M. S. (1982). The determination of hydroxyl by infrared absorption in quartz, silicate glasses and similar minerals. *Bulletin of Mineralogy* **105**, 20–29.

Peslier, A. H. & Luhr, J. F. (2006). Hydrogen loss from olivines in mantle xenoliths from Simcoe (USA) and Mexico: Mafic alkalic magma ascent rates and water budget of the sub-continental mantle. *Earth and Planetary Science Letters* **242**, 302–319.

Rossman, G. R. (1988). Vibrational spectroscopy of hydrous components. In: Hawthorne, F. C. (ed.) *Spectroscopic Methods in Mineralogy and Geology*. Washington, DC: Mineralogical Society of America, pp. 183–206.

Sambridge, M., Fitz Gerald, J. D., Kovács, I., O'Neill, H. St. C. & Hermann, J. (2008). Quantitative IR spectroscopy with unpolarized light, Part I: Physical and mathematical development. *American Mineralogist* (in press).

Takanami, T., Sacks, I. S. & Hasegawa, A. (2000). Attenuation structure beneath the volcanic front in northeastern Japan from broad-band seismograms. *Physics of the Earth and Planetary Interiors* **121**, 339–357.

Tan, B. H., Jackson, I. & Fitz Gerald, J. D. (1997). Shear wave dispersion and attenuation in fine-grained synthetic olivine aggregates: preliminary results. *Geophysical Research Letters* **24**, 1055–1058.

Tan, B. H., Jackson, I. & Fitz Gerald, J. D. (2001). High-temperature viscoelasticity of fine-grained polycrystalline olivine. *Physics and Chemistry of Minerals* **28**, 641–664.

Turner, F. J. (1942). Preferred orientation of olivine crystals in peridotites, with special reference to New Zealand examples. *Transactions of the Royal Society of New Zealand* **68**, 570–98.

Walker, A. M., Hermann, J., Berry, A. J. & O'Neill, H. St. C. (2007). Three water sites in upper-mantle olivine and the role of titanium in the water-weakening mechanism. *Journal of Geophysical Research* **112**, B05211, doi:10.1029/2006JB004620.

Wood, B. L. (1972). Metamorphosed ultramafites and associated formations near Milford Sound, New Zealand. *New Zealand Journal of Geology and Geophysics* **15**, 88–128.

Yoshino, T., Nishihara, Y. & Karato, S. (2007). Complete wetting of olivine grain boundaries by a hydrous melt near the mantle transition zone. *Earth and Planetary Science Letters* **256**, 466–472.

Zhao, D., Hasegawa, A. & Horiuchi, S. (1992). Tomographic imaging of P and S wave velocity structure beneath northeastern Japan. *Journal of Geophysical Research* **97**, 19909–19928.

Zhao, Y. H., Ginsberg, S. B. & Kohlstedt, D. L. (2004). Solubility of hydrogen in olivine: dependence on temperature and iron content. *Contributions to Mineralogy and Petrology* **147**, 155–161.